All-Optical Phase Memory Circuit Based on Two Coupled Lasers and External Optical Injection

Tuomo von Lerber, Vladimir S. Lyubopytov, Lauri Ylinen, Matti Lassas, and Franko Küppers

***Abstract*—We propose a volatile static all-optical memory capable of storing phase information of a slowly-varying electric field. The scheme and its realization (a memory circuit) are based on two mutually coupled lasers subject to external optical injection. The proposed circuit has a single optical input for write and hold operations and two opposite-sign outputs for reading the memory. The proposed circuit operates with a single wavelength of light, a single direction of propagation, and without a need to switch the state of polarization. We prove mathematically that the proposed arrangement has equilibrium points that may discreetly quantify and store the phase in a bistable manner. The circuit is studied numerically for solid-state and semiconductor lasers with zero and non-zero linewidth enhancement factors, respectively. Simulations based on a rate equation system confirm the essential findings. Using typical parameters of a semiconductor laser and optimizing for a possibly wide range of operation, the write-read operations were simulated using PRBS-9 at the rate of 1 Gb/s with negligible errors. The proposed circuit will enable integrated memory implementations for future all-optical signal processing and computing systems.**

***Index Terms*—Optical memory, semiconductor lasers, coupled oscillator systems, optical injection locking, optical computing.**

I. Introduction

THE von Neumann bottleneck is a limitation of computers that arises from the fact that the central processing unit (CPU) can perform more instructions per second than data can be transferred from memory. A mitigation to the bottleneck is to use a fast cache memory near the processing cores.

A potential next step in the increase of execution speed is to use all-optical computing principles. That is, utilizing logic gates and memory circuits that process and store light, not charged particles. Using photons instead of electrons as information carriers bears a promise of higher data transmission rates at the bus between the CPU and memory. Here, we investigate a memory circuit that stores binary information and could be accessible with low latency.

Since the first optical memory setup was reported [1], several theoretical approaches and realizations have been proposed and experimentally demonstrated, including those based on photonic integrated circuits (PICs) [2], [3], [4], [5]. Initially, optical flip-flop and memory devices were developed to store packet-level information, such as resolving packet headers. The main approaches include the use of optical delay lines [6], slow-light optical buffers [7], [8], and semiconductor optical amplifier Mach-Zehnder interferometer (SOA-MZI) based flip-flops [9]. In the past decade, development has progressed toward bit-level optical storage, primarily due to advances in photonic integration technologies [10], [11], [12], [13].

The requirements for optical transistors as fundamental optical computing elements were formulated in [14]. The same rules can be applied to more complex computing elements, such as optical logic gates and optical memory circuits. These requirements include:

1) Cascadability, i.e., compatibility of the input and output wavelengths and shapes of beam and pulse.
2) Fan-out capacity, i.e., the output of one stage should be sufficient to drive the inputs of at least two subsequent stages.
3) Logic-level restoration, i.e., cleaning up the logic signal from distortions when propagating through the system.
4) Input/output isolation, i.e., separation of the input and output signals.
5) Absence of critical biasing, i.e., tolerance to the operating parameters.
6) Logic level independence of transmission losses that may differ due to varying signal paths.

Moreover, the memory bandwidth, energy efficiency, integration density, and access time are of particular interest for optical memories [15].

Analogously to the electronic memory circuits, optical bit-level memories can be divided into two categories: dynamic and static, depending on the presence or absence of the required memory state refreshing, respectively. Various schemes have been studied for optical dynamic memory capabilities, such as optical buffers based on recirculating loops [16], bistable systems based on absorption and transparency [17], [18], and electroluminescence [19] in a rare-earth-doped medium.

Manuscript received 3 June 2022; revised 11 January 2023; accepted 17 January 2023. Date of publication 23 January 2023; date of current version 6 February 2023. This work was supported (ML and LY) by the Finnish Centre of Excellence in Inverse Modelling and Imaging and Academy of Finland under Grants 284715 and 312110. *(Corresponding author: Lauri Ylinen.)*

Tuomo von Lerber, Lauri Ylinen, and Matti Lassas are with the Department of Mathematics and Statistics, University of Helsinki, 00014 Helsinki, Finland (e-mail: tuomo.lerber@iki.fi; lauri.ylinen@helsinki.fi; matti.lassas@helsinki.fi).

Vladimir S. Lyubopytov is with the Center for Photonic Science and Engineering, Skolkovo Institute of Science and Technology, 121205 Moscow, Russia, and also with the Ufa University of Science and Technology, 450076 Ufa, Russia (e-mail: v.lyubopytov@skoltech.ru).

Franko Küppers is with the Wyant College of Optical Sciences, University of Arizona, Tucson, AZ 85721 USA (e-mail: franko.kueppers@optics.arizona.edu).

This article has supplementary material provided by the authors and color versions of one or more figures available at https://doi.org/10.1109/JSTQE.2023.3239167.

Digital Object Identifier 10.1109/JSTQE.2023.3239167

The known static memory implementations are based on optical bistability with two discrete states and have been demonstrated using the following phenomena: i) cross-phase modulation (XPM) in the two coupled SOA-MZI switches [20], [21], [22], [23], or cross-gain modulation (XGM) in the two coupled SOAs [5], [24], or XPM due to polarization-dependent gain saturation in the two coupled strained SOAs [25], all with the data encoding in the wavelength domain; ii) light recirculation in a feedback loop with an SOA-MZI [26], [27], [28]; iii) gain quenching mechanism in two [29], [30], [31] or three [32] coupled lasers in master-slave configuration, or in the cavities sharing the same SOA [33]; iv) nonlinear absorption and the resulting output power bistability in a laser diode with saturable absorber (referred to as a bistable laser diode – BLD) [34], where optical set/reset functions are realized by a combination of a BLD with nonlinear directional coupler [35] or using cross-gain saturation between two lasing modes in a multimode interference BLD [36], [37]; v) hysteresis loop in the laser output power vs. the injected power, caused by nonlinear dynamics of an injection-locked Fabry-Perot laser diode [38], or a DFB laser [39], or a system of mutually coupled DFB laser and SOA with external injection [40]; vi) lasing direction bistability in a semiconductor ring [4], [41], or microdisk [2] laser, or two coupled ring lasers [42]; vii) carrier-induced refractive index blue-shift and corresponding hysteresis response in an injection-locked photonic crystal (PhC) laser [43], [44], [45] or PhC nanocavity [3], [46], [47], [48]; viii) polarization bistability due to cross-gain saturation in an injection-locked Vertical-Cavity Surface-Emitting Laser (VCSEL) [49], [50], [51], [52].

Still, a non-volatile optical memory has been realized by absorption modulation in phase-change materials (PCM) [53], [54]. The phase-state transitions in PCM rely on Joule heating, which limits the lower bound of the write/erase pulse duration and energy by the range of several nanoseconds and several picojoules, respectively. Consequently, current PCM-based optical memory realizations resemble more all-optical counterparts of the traditional erasable programmable read-only memory rather than random access memories.

Bistable optical memory arrangements have been demonstrated with injection-locked lasers utilizing the following physical phenomena:

1) Wavelength [43], [44], [45], [55], [56],
2) State of polarization [49], [50], [51], [52],
3) Laser output power [38], [57], and
4) Propagation direction [2], [4], [41], [42].

The first approach provided operation speeds up to 10 Gb/s [45] with a comparably small footprint and energy consumption, and the technology was claimed to be ready for high-density integration [3]. However, this approach implies that the input and output signals are at different wavelengths [43], [44], [45], or the output signal is wavelength-encoded [43], [44], [45], [55], [56]. This can be desirable for all-optical wavelength routing systems but impairs cascadability in optical computing applications — a non-negotiable requirement of complex logic circuits. The second approach involves two orthogonal states of polarization, and therefore relies on optical medium of sufficiently low birefringence to achieve a polarization bistability. To fulfill this condition, usually VCSELs are used; yet, the vertical emission may complicate large-scale planar integration on existing photonic platforms. The third approach is advantageous that it uses intensity domain signal encoding; however, it also requires the input signal (i.e., the set and reset pulses) at wavelengths different from the laser output signal. The last approach, typically implemented using micro-ring or micro-disk lasers, has demonstrated a small footprint compared to other memory circuit schemes, low switching energy (down to 2 pJ [42]), and fast switching times (down to 20 ps [42]). The different memory states, in this case, can be distinguished by power levels at the two laser outputs, which is also equivalent to the data encoding in the intensity domain. However, the last two approaches use separate set and reset input ports for the writing procedure (i.e., working as an SR-latch), thus requiring an additional logic gate stage.

We propose utilizing the phase of an optical signal for encoding information, with ‘zero’ and ‘one’ represented by different phase values in reference to a global master oscillator signal. In this case, the input (write) and output (read) signals are at the same constant wavelength, polarization, and direction of propagation. The proposed scheme can be considered a D-type latch. Phase encoding of logic states is convenient in optical computing applications due to the requirements mentioned above [14], which we will analyze in the Discussion below. Consequently, the proposed scheme opens new opportunities for complex computing and signal processing architectures, similar to conventional electronics. Moreover, phase modulation with coherent detection is known to provide additional SNR gain compared to amplitude modulation (up to 3.2 dB at 1 b/symbol spectrum efficiency and bit-error rate (BER) of 10^{-9} [58]).

To create a system with optical phase bistability, we employ two coupled optical oscillators (lasers) in the optical injection locking (OIL) regime, which implement two normalization operations [59]. The dynamical behavior of the coupled laser arrays with external injection locking has been extensively modeled and analyzed in the literature (see [60] and references therein). Usually, these systems are investigated for the conditions providing stable continuous wave (CW), oscillatory and chaotic operation states. In our approach, the task is more specific. The system of two coupled OIL lasers should be stable and provide optical phase memory functionality, i.e., keep the different phase states once written. This requirement, as simulation shows, narrows down the operation regions in the system’s parameter space; however, they still exist for both ideal and semiconductor lasers (i.e., with zero and non-zero linewidth enhancement factors α, respectively).

Here, we intentionally do not link our memory circuit concept and numerical modeling parameters to any specific laser type because the circuit can be implemented with various possible lasers, including integrated InGaAsP/InP edge-emitting lasers, VCSELs, nanolasers, or photonic crystal nanocavity lasers. The latter has been demonstrated as a promising solution in terms of size and energy consumption [43], [44],

[45]. The study of specific layout options and analysis of footprint and power consumption are beyond the scope of this Paper.

II. Operating Principle

A. Concept of a Bistable Circuit

The operation of a bistable circuit can be mathematically described with a pair of coupled equations as

$$z_1 = \left(e^{i\pi} z_2 + b_1\right)^0,\ z_2 = \left(e^{i\pi} z_1 + b_2\right)^0, \tag{1}$$

where z_k is the output amplitude of the nonlinear element $k \in \{1, 2\}$, b_k is the external bias, and $z_k, b_k \in \mathbb{C}$. The normalization operation is denoted as $z^0 \equiv z/|z|$. The circuit of (1) has solutions

$$\text{State \#1: } (z_1, z_2) = \left(e^{+i\pi/3},\ e^{-i\pi/3}\right),$$

$$\text{State \#2: } (z_1, z_2) = \left(e^{-i\pi/3},\ e^{+i\pi/3}\right),$$

when the bias $b_1 = b_2 = 1$. That is, in both equilibrium states, the nonlinear elements output a constant amplitude of one, and a phase that can be one of the two possible values. The equations have no time dependence, and the state will not change if the biases remain constant. Consequently, the circuit of (1) may retain its phase state indefinitely and serve as a memory, or a latch, assuming there would be a way to flip between the states purposefully.

We recently showed in [59], [61] that a weakly injection-locked laser can perform the required normalization operation of (1). For this Paper, we study the bistable circuit with a system of rate equations (Appendix A) and provide a rigorous mathematical analysis of the circuit (Appendix B), albeit using a simplified laser model. We show the possibility for equilibrium points where the phase will be quantified and retained indefinitely, including the pair of states $(e^{\pm i\pi/3},\ e^{\mp i\pi/3})$ when $b = 1$. Depending on the relative strength of the external bias b, the system may have five different sets of equilibria. Some of these steady-state solutions are trivial (e.g., when the injection is strong, or nil), but we also found solutions with meaningful phase differences for two-state phase information encoding.

An idealized model of the phase memory circuit is illustrated in Fig. 1(a) that shows the mutual coupling of the two nonlinear elements $\{\mathrm{L1}, \mathrm{L2}\}$ (rectangular symbols) and the linear operations of phase shift and addition (round symbols). In other words, each nonlinear element receives a signal that combines the bias and the opposite amplitude of the other element's output.

When the nonlinear elements of the circuit are replaced with mutually coupled lasers, the circuit can be described purely with optical components. Two possible realizations are schematically illustrated in Figs. 1(b) and (c) for the ring and linear cavity lasers, respectively.

A notable difference between the physical and idealized models is time constants, or the lack thereof. The idealized model assumes instantaneous interaction between the nonlinear elements and equally instantaneous normalization operations.

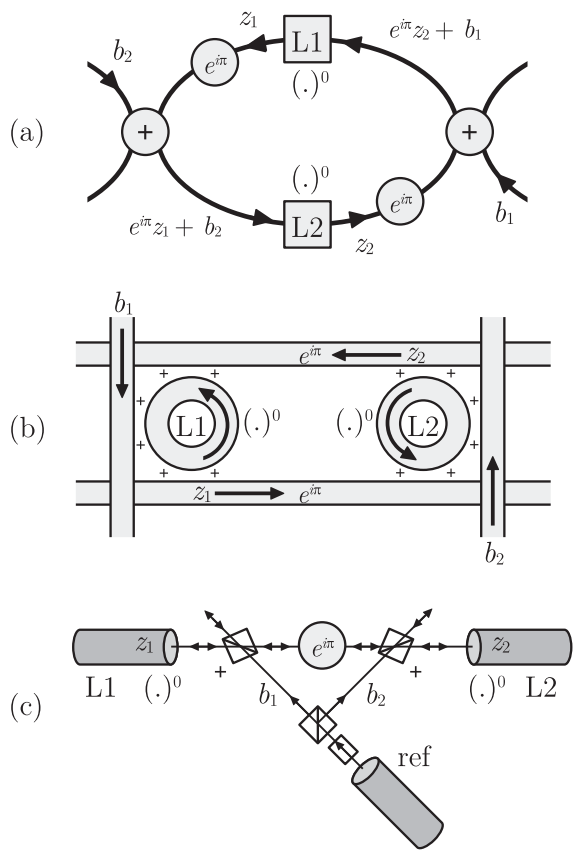

Fig. 1. Operating principle of the optical memory circuit. (a) A nonlinear element L1,2 performs the normalization operation $(\cdot)^0$ and outputs the complex amplitude $z_{1,2}$ that experiences the phase-shift of π and is combined with the bias $b_{1,2}$. (b) A possible realization using ring lasers L1 and L2. The circuit topology follows the example above. The small plus signs around the rings symbolize the evanescent coupling between the waveguides and the laser rings. (c) An optical memory based on linear cavity lasers L1,2. The bias $b_{1,2}$ is generated by a reference laser whose output is split in two. Here, the reference signal is assumed to have sufficiently high degree of coherence. The cubical beam combiners perform the required addition operations $(+)$.

In addition to the rigorous mathematical proof, we will explore the memory circuit properties under various operating conditions while increasing the level of realism and complexity of the system. The numerical modeling will assume non-instantaneous normalization operations using rate equations (see Appendix A and [59], [61], [62]) and the existence of a delay in signal propagation (i.e., distance) between the lasers. In other words, each laser is injected with a field that is the history of the other laser output combined with external injection. First, we will model the circuit with zero linewidth enhancement factor $(\alpha = 0)$, i.e., a solid-state laser, such as Nd:YAG or alike. Next, we will assume a semiconductor laser with non-zero linewidth enhancement factor $\alpha \approx 3$, which is known to potentially destabilize mutually connected semiconductor lasers [60].

B. Operating Scheme

Simulations of the two-laser phase memory ran on arrangement schematically depicted in Fig. 2. Here, light from the external master laser is injected with the power coupling efficiency κ_{inj} at a fixed linear state of polarization, aligned along

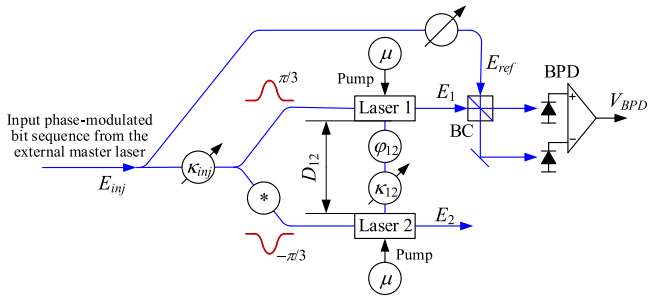

Fig. 2. Schematic illustration of the optical phase memory circuit (here * denotes opposing the injected signal phase, i.e. complex conjugation; BC – beam combiner; BPD – balanced photodiode).

a possible polarization axis of the coupled lasers (assumed now x-axis). The lasers are identically pumped with the normalized pumping rate μ. Optical injection from the external master laser may have the frequency detuning relative to the free-running frequency of the coupled slave lasers: $\Delta\nu_{inj} = \nu_{inj} - \nu_{fr}$. The power coupling efficiency between the coupled lasers is κ_{12}. The phase-shift ϕ_{12} between the coupled lasers consists of a constant term ϕ_0, which is set to π by default (unless mentioned otherwise), and a term proportional to the frequency detuning and the delay in signal propagation between lasers (see Appendix A):

$$\phi_{12} = \phi_0 + 2\pi\Delta\nu_{inj}\tau_{12}. \tag{2}$$

The system is (bi)stable under suitable operating conditions and will ideally retain a state as long as the external injection is constant (static nature of the memory). A short phase perturbation serves as an event that erases and writes a new state into the memory (volatile nature of the memory). Theoretically, it is enough to subject only one laser to the write event. However, simulations showed that the system settles faster and more reliably if the write event is injected simultaneously on both lasers with opposing information states. For instance, assuming $b = 1$, if Laser 1 is subject to optical injection with the electric field phase of $e^{+i\pi/3}$, then Laser 2 should be subjected to injection with the phase of $e^{-i\pi/3}$. The numerical model assumes the carrier number decay rate γ of 2.0 ns^{-1} and the cavity electric field decay rate γ_c of 500 ns^{-1} for both lasers.

The phase-encoded memory state is read with a standard coherent receiver arrangement [63] that consists of a beam combiner (BC) and a pair of balanced photodiodes (BPD) (see Fig. 2). The x-polarized output field E_1 of the Laser 1 is combined in the BC with the x-polarized reference signal E_{ref} from the external master laser. The differential output provides a steady phase-to-power converted signal when the lasers are phase-locked.

III. Numerical Modeling

A. Model Description

The differential equation system of (9) and (10) of Appendix A was integrated numerically to find stable regions in the system parameter space. For this, we used the delayed differential equation (DDE) solver in Julia [64], [65] with

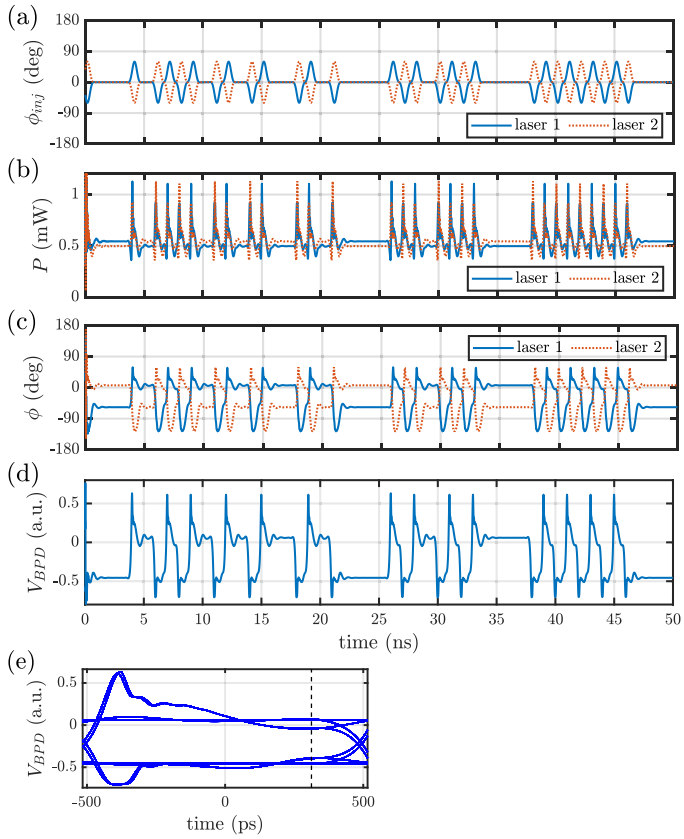

Fig. 3. Trace analysis of the system signals. (a) Fragment of the injected input signal phases, (b) the corresponding output powers and (c) phases of Lasers 1 and 2, (d) the BPD output signal, and (e) eye-diagram. The used system parameters: $\alpha = 3$, $D_{12} = 3.0$ mm ($\tau_{12} \approx 37.03$ ps), at the point $\Delta\nu_{inj} = -30.3$ GHz, $\kappa_{inj} = -10.1$ dB. Dashed line in the eye-diagram shows the middle of the 'read' time period.

post-processing and analysis of the calculated output traces using MATLAB. In order to simulate possibly realistic operation conditions, we used pseudo-random binary sequence input (PRBS-9, consisting of $2^9 - 1$ bits), each bit slot containing 'write' and 'hold' periods. The intensity of injection was kept constant to provide the required locking. The phase of the optical injection was set and changed in the spirit of encoding used in coherent communications. The phase was kept to "zero" if the bit value did not change relative to the previous bit. Otherwise, during the "write" part, the injected signal phase was temporarily changed to the opposing $\pm\pi/3$ or $\mp\pi/3$ for the lasers 1 and 2, respectively. Here the upper and lower signs represent the input bit of "one" or "zero," respectively. In our simulations, the length of the 'write' period was 38% of the bit slot duration, and the 'hold' period (where the bit slot payload remains stored and can be read) occupied the rest 62% of the bit slot duration. We optimized this proportion for possibly large eye-opening within the 'read' period. Then, in order to smooth the input signal and make it implementable in real systems, we limited the bandwidth by a raised-cosine filter of $1/(2T_w)$, where T_w is the duration of the 'write' pulse, and using a roll-off factor of 1.0 that provided optimal performance. Fig. 3(a) shows an example of the injected signal phase at the bit rate of 1 Gb/s.

At the system output, after the field E_1 of Laser 1 was combined with the reference signal E_{ref}, the output from the balanced photodiode (BPD) obeyed the relation:

$$V_{BPD} \sim |-iE_1 + E_{ref}| \cdot |E_1 - iE_{ref}| \times \cos\left(\arg\left(-iE_1 + E_{ref}\right) - \arg\left(E_1 - iE_{ref}\right)\right). \quad (3)$$

Fig. 3(b)–(e) show the output power and phase of the lasers, the corresponding voltage trace, and the eye diagram at the BPD, respectively.

To analyze the dynamic behavior and the memory function, we plot 2-D maps in the parameter spaces of '$\Delta\nu_{inj}$ vs. κ_{inj}' and '$\Delta\nu_{inj}$ vs. D_{12}', where D_{12} is the inter-laser distance (i.e., the waveguide length between the two coupled slave lasers), which is proportional to the delay in signal propagation time τ_{12} (here, we assume the group refractive index of the waveguide between lasers $n_g = 3.7$, typical for InP-based integration platforms). While sweeping over the dimension of inter-laser distance, the phase shift between the lasers remains defined by (2). Theoretical BER is calculated as:

$$BER = \frac{1}{2}\mathrm{erfc}\left(\frac{Q}{\sqrt{2}}\right), \quad (4)$$

where Q stands for the Q-factor:

$$Q = \frac{\left|\langle V^1_{BPD}\rangle - \langle V^0_{BPD}\rangle\right|}{(\sigma^1 - \sigma^0)}, \quad (5)$$

and V^1_{BPD} and V^0_{BPD} are the respective output voltage levels of 'one' and 'zero' bits. The mean values of output voltage levels and corresponding standard deviations σ^1 and σ^0 are calculated over the 'read' period for all the bits in the PRBS under consideration. Only those regions were analyzed for BER where $\min\{V^1_{BPD}\} - \max\{V^0_{BPD}\} > 0$. Non-analyzed regions are colorless on BER maps.

Coherent optical systems are susceptible to changes in internal or external variables. The same applies to the proposed memory circuit that bears sensitivity in a detuning between the injected and the free-running laser frequencies. However, the circuit has some in-built robustness in the operational bias condition. Proposition 1 (Appendix B) suggests that the relative external bias b (16) determines the system behavior. The bias depends on the pumping rate μ, the effective injected field $\kappa_{inj}E_{inj}$, and the inter-laser coupling efficiency κ_{12}. In practice, the coupling efficiency of the external field κ_{inj} is usually limited by the laser cavity design. Thus, should we desire to keep the bias, we can compensate for this limitation by adjusting the value of κ_{12}, or vice versa.

The simplified laser model of Appendix B assumes operation in the vicinity of the threshold pump current. The simulations indicate proper operation also at the higher end of the pumping rate. As numerical results show below, the pumping range $\mu = 1.3$–1.7 provided sufficient operational freedom. Also, from a practical point of view, such a range is reasonable for maintaining low power consumption. A higher pumping rate is possible, yet this increase does not yield substantial performance enhancement.

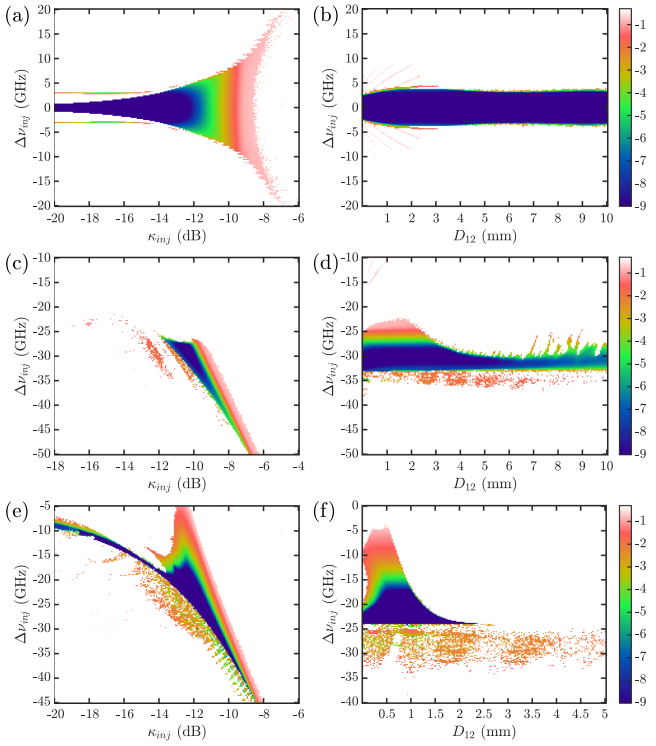

Fig. 4. Simulated BER maps over the varying coupling strength of the injection κ_{inj} (first column) and inter-laser distance D_{12} (second column). The sub-figures (a) and (b) illustrate the case $\alpha = 0$, and sub-figures (c)– (f) when $\alpha = 3$. Colorless white regions surrounding the Arnold tongues refer to parameter space where the coherently detected signal eye was closed and no BER could be determined.

Finally, the constant part of the optical phase-shift between lasers ϕ_0 was optimized to provide a possibly wide operation tolerance to the external injection parameters.

B. Numerical Modeling Results

A collection of BER maps is shown in Fig. 4. The first and second columns (sub-figures (a), (c), (e), and (b), (d), (f)) illustrate the operating regions where the power coupling efficiency κ_{inj} and the inter-laser distance D_{12}, respectively, are varied over the injection frequency detuning $\Delta\nu_{inj}$. The bit rate was 1 Gb/s at all instances.

Fig. 4(a), (b) show the output maps of a non-semiconductor Laser 1 ($\alpha = 0$) with inter-laser coupling κ_{12} of -17 dB, phase-shift ϕ_0 of π, and normalized pumping μ of 1.5.

The sub-figure (a) shows the case with a fixed inter-laser distance D_{12} of 3.0 mm, but varied injection coupling κ_{inj}. The operational parameter region is centered around zero frequency detuning of the external injection, manifesting a simple Arnold tongue of phase-locking. The BER map indicates the tolerance of 4 dB $\times$ 5.5 GHz to the external injection parameters $\kappa_{inj} \times \Delta\nu_{inj}$ (at the BER level of 10^{-7}). Referring to the simplified mathematical model of the memory circuit (Appendix B), the results confirm Proposition 1. As the simplified model predicts, the increase of the injection coupling efficiency κ_{inj} results in diminished phase difference (closing eye) between the

two steady states. In addition, the numerical modeling shows that the increase also provides a wider tolerance to the injection frequency detuning. The finding is further corroborated in Supplementary Figures showing the system remains stable over a wider parameter range under strong coupling, yet, without memory function (see Figs. S1, S3, S5 sub-figures c,d).

The corresponding BER map of Fig. 4(b) is calculated with a fixed injection coupling κ_{inj} of -13.2 dB, yet, with varying inter-laser distance D_{12}. The system is stable and provides memory functionality with similar behavior within a reasonably wide range of distances between the coupled lasers. The injection detuning may vary over the range of 6.1 GHz, centered around 0 GHz.

As known, a semiconductor laser with linewidth enhancement factor $\alpha > 0$ shifts the stable phase-locking region to the negative detuning values and makes the injection-locked laser otherwise prone to harmonic oscillations or chaotic behavior [66]. Fig. 4(c), (d) shows the modeling results of the memory circuit with $\alpha = 3$, which is typical for multiple quantum well (MQW) lasers [67]. In these simulations, we used the following parameter values: inter-laser coupling κ_{12} of -19 dB, phase-shift ϕ_0 of 1.24π, and normalized pumping μ of 1.3. As evident, the central stable detuning value shifts to the neighborhood of -31 GHz.

The sub-figure (c) shows the case with the same fixed inter-laser distance D_{12} of 3.0 mm as in sub-figure (a). Now, the memory functions within a relatively narrow stripe of approximately 0.9 dB $\times$ 5 GHz (at the BER level of 10^{-7}) centered at $\kappa_{inj} = -10.1$ dB and $\Delta\nu_{inj} = -30.3$ GHz.

The corresponding varying inter-laser distance BER map (d) is calculated with the fixed injection coupling κ_{inj} of -10.1 dB. As in the previous case, the system exhibits agnosticism toward the changing distance until the BER space tapers out for distances greater than 3 mm.

For practical purposes, we naturally aim for a semiconductor laser memory circuit with a possibly wide operations range, yet, with a minimal footprint. To this end, we sought a new operations point with decreased inter-laser distance D_{12} of 0.5 mm and conducted simulations using the following parameter values: inter-laser coupling κ_{12} of -19 dB, phase-shift ϕ_0 of 1.33π, and normalized pumping μ of 1.5.

Sub-figure (e) shows an enlarged functional BER map with substantial improvement over the sub-figure (c). The functional region is centered around $\kappa_{inj} = -12.4$ dB and $\Delta\nu_{inj} = -20$ GHz.

The accompanying BER sub-figure (f) exhibits a widened tolerance to frequency detuning (up to 7.5 GHz) when the fixed injection coupling κ_{inj} is -12.4 dB. The inter-laser distance working region is now limited to approximately $D_{12} < 1.5$ mm, which is more than enough for most integrated optical implementations.

As mentioned in Section III-A above, the system tolerates the pumping rate μ within a relevant range. Supplementary Fig. S7 shows the BER maps, corresponding to the previously discussed cases and shown in Fig. 4(a), (e), yet, for the pumping rate μ values of 1.3 and 1.7.

The simulations show decent robustness of the proposed circuit to the asymmetry of the coupled lasers parameters. First, we introduced up to $\pm 20\%$ mismatch in pumping rates μ_1 and μ_2 for the case of ideal lasers ($\alpha = 0$), and up to $\pm 7\%$ mismatch for semiconductor lasers ($\alpha = 3$). The stable memory operating region shrank as if both lasers were pumped at the lower value of the μ_1 and μ_2 rates. Only a further increase in the pumping rate mismatch degraded the results rapidly. Second, we obtained similar results for the mismatch of cavity electric field decay rates $\gamma_{c,1}$ and $\gamma_{c,2}$, which incorporate the laser cavity losses and geometric properties. The circuit was resilient up to a mismatch of about $\times 2$ for $\alpha = 0$, and up to $\pm 5\%$ for $\alpha = 3$. Until then, the memory circuit would operate adequately, shrinking the operable parameter region as if both lasers were having the same lower γ_c.

We tested cascadability as follows. First, we simulated the memory circuit and stored its output reading phase states. Then we ran a new simulation where we applied the output phase states of the previous run as inputs, thus having an effective feed-forward configuration. The numerical modeling confirmed the operation. Here, the phase shift between the circuits was controlled such that the "zero" and "one" states had symmetrical opposite phase values (see Supplementary Fig. S8). In this test, the noise accumulation was neglected. Assuming the results hold also for a physical circuit, the modulation format will be preserved even through a long cascade. The result agrees with our prediction that the mutually coupled oscillator system has energy minima and will always gravitate toward these states and indicates that the circuit bears a critically important property: the restoration of logic levels.

In summary, memory operation can be achieved using two interconnected lasers and external bias. Non-surprisingly, the parameter space is more generous when $\alpha = 0$, but semiconductor lasers will function when the inter-laser phase is adjusted according to (2). Importantly for practical applications, and especially for integrated optical designs, the inter-laser distance D_{12} can be chosen liberally.

IV. Discussion and Conclusions

We proposed an all-optical static memory circuit based on the phase bistability of two mutually coupled lasers and external bias, whose perturbations can realize write operations. Referring to cascadability and accompanying properties of an implementable optical computing system [14], the present scheme benefits from the same wavelength, the same state of polarization, the same direction of propagation, and an unaltered information encoding format at the input and the output. Also, the simulation results suggest restoration of the logic states in a cascade.

The circuit inherently provides two outputs, which may drive two subsequent logic elements — thus fulfilling the requirement of fan-out. Also, depending on the optical system design, the laser output may counter losses of the remaining system and restore the optical power levels.

Necessary for practical designs, the circuit is tolerant to many parameters, such as inter-laser distance, given that the phase can be adjusted. Inter-laser coupling efficiency and coupling of the external bias must be accommodated within a few decibels,

and frequency detuning of the external bias should usually lie within a range of a few GHz. Noteworthy, the operation parameter region will widen by decreasing the inter-laser distance, naturally improving the system integration density. Finally, one of the main advantages of the proposed scheme is its relative independence of transmission losses due to phase encoding.

The proposed memory circuit is envisioned to provide high-frequency operation in the baseband range of tens of gigahertz. In our numerical model, we used the bit rate of 1 Gb/s; however, the normalization operation at the speed of 10 Gb/s was experimentally demonstrated even with a bulk Fabry-Pérot laser [68], and with a transition to micro- and nano-scale integrated lasers will likely increase the bandwidth further. We believe the proposed circuit is suitable for applications where high throughput is crucial, such as photonic counterparts of conventional electronic cache or random-access memories.

Regardless of the chosen laser type and properties of the optical medium, practical implementation of a functioning circuit will require specialized know-how. As an example, single-mode operation of a laser is rarely a coincidence, but a result of careful design and fabrication, albeit the external optical injection is assumed to assist in our case. For instance, a ring laser-based circuit will likely require unidirectional propagation of light. To quench the undesired direction of propagation, some mitigation is likely needed. An option would be to use a broadband multimode interference reflector (MIR) or a Bragg reflector. Even more, reflections elsewhere from the optical system must be controlled and possibly minimized to ensure reliable operation of the memory.

Regarding practical implementation and projected circuit characteristics, the proposed circuit's storage density and power consumption will strongly depend on the used type of lasers and the properties of the photonic integration platform. Therefore, we must leave the quantitative assessment for further elaboration. However, considering an electronically-pumped continuous-wave room-temperature semiconductor laser with sub-wavelength dimensions [69], the circuit storage density may achieve the magnitude of one wavelength per bit. That said, the memory circuit's size will also be determined by the optical interconnects between its elements and the power dissipation constraints.

Compared to the existing optical memory schemes, the proposed circuit uses phase encoding of logic states instead of intensity encoding. Thus, the involved lasers will work with constant energy feeding. The transient intensity peaks arising when switching the logic states (see Fig. 4(b)) are a short parasitic effect. The switching energy will be defined mainly by the external phase modulation procedure. The energy consumption of the memory circuit will be determined by the pumping energy of the involved lasers (the shared external master and two coupled slave lasers). Assuming, for instance, the properties of [69], normalized pumping rate $\mu = 1.5$, and the information rate of 25 Gb/s, the constant energy consumed by the lasers will be about 1 pJ/bit for supporting "write," "hold," and "read" operations. Yet, the overall power consumption of the circuit will also depend on the realization of interconnects between its elements.

In this Paper we have increased the level of realism step by step, starting from a simple pair of coupled equations and ending up to use delay-differential equation system with non-zero linewidth enhancement factor. A possible next step on this path would be to use stochastic differential equations to model spontaneous emission and fluctuations in the number of carriers.

The proposed circuit appears feasible for integrated implementation. The passive and active building blocks used in the proposed memory circuit are currently available in the process development kits (PDK) of commercially available InP/InGaAsP-based platforms. Novel nanophotonic integration platforms are desired to improve energy efficiency and footprint further.

Appendix A
Laser Rate Equations

We model a laser under external optical injection with rate equations [59], [61], [62]:

$$\gamma_c^{-1}\dot{E}^{\omega_{fr}}(t) = (1+i\alpha)(N(t)-1)E^{\omega_{fr}}(t) + u(t), \tag{6a}$$

$$\gamma^{-1}\dot{N}(t) = -N(t)(1+|E^{\omega_{fr}}(t)|^2) + \mu. \tag{6b}$$

Here $E^{\omega_{fr}}$ is the complex-valued slowly varying amplitude of a linearly polarized complex electric field $\mathcal{E}$,

$$\mathcal{E}(z,t) = \mathrm{Re}\left(E^{\omega_{fr}}(t)e^{-i(kz-\omega_{fr}t)}\right), \tag{7}$$

where ω_{fr} is the angular free-run frequency of the laser, z is the spatial variable, k is the wave number, u is the external injection, and N is the normalized difference of the sums of the upper and the lower state populations. The dot-operator denotes time derivative $\dot{x} \equiv \frac{dx}{dt}$, α is the linewidth enhancement factor, γ is the decay rate of the total carrier number, γ_c is the decay rate of the electric field in the cavity, and μ is the normalized injection current (1 at the threshold and about 3 at 1 mW output of a typical vertical-cavity surface-emitting laser).

Laser output signal (7) has the power defined as:

$$P(t) = \frac{1}{2}\left(E^{\omega_{fr}}(t)\cdot E^{\omega_{fr}}(t)^*\right), \tag{8}$$

where * denotes the complex conjugate.

The memory circuit consists of two mutually coupled lasers that are injected externally. Both lasers are assumed to share common values for the parameters α, γ, γ_c, and μ. The coupled rate equations for the lasers 1 and 2 are

$$\gamma_c^{-1}\dot{E}_1^{\omega_{fr}}(t) = (1+i\alpha)(N_1(t)-1)E_1^{\omega_{fr}}(t) + u_1^{\omega_{fr}}(t), \tag{9a}$$

$$\gamma^{-1}\dot{N}_1(t) = -N_1(t)(1+|E_1^{\omega_{fr}}(t)|^2) + \mu, \tag{9b}$$

$$\gamma_c^{-1}\dot{E}_2^{\omega_{fr}}(t) = (1+i\alpha)(N_2(t)-1)E_2^{\omega_{fr}}(t) + u_2^{\omega_{fr}}(t), \tag{9c}$$

$$\gamma^{-1}\dot{N}_2(t) = -N_2(t)(1+|E_2^{\omega_{fr}}(t)|^2) + \mu, \tag{9d}$$

with

$$u_1^{\omega_{fr}}(t) = \kappa_{12}e^{i\phi_{12}}E_2^{\omega_{fr}}(t-\tau_{12}) + \kappa_{1,inj}E_{1,inj}(t)e^{it\Delta\omega_{inj}}, \tag{10a}$$

$$u_2^{\omega_{fr}}(t) = \kappa_{21}e^{i\phi_{21}}E_1^{\omega_{fr}}(t-\tau_{12}) + \kappa_{2,inj}E_{2,inj}(t)e^{it\Delta\omega_{inj}}, \tag{10b}$$

where $E_{1,inj}$ and $E_{2,inj}$ are the slowly varying amplitudes of external sources that have the frequency ω_{inj}, and $\Delta\omega_{inj} = \omega_{inj} - \omega_{fr}$ is the angular frequency deviation from the external source ($\Delta\omega_{inj} = 2\pi\Delta\nu_{inj}$, where $\Delta\nu_{inj}$ is the frequency detuning). The effect of electric fields $E_1^{\omega_{fr}}$ and $E_2^{\omega_{fr}}$ are delayed by constant τ_{12} and multiplied with complex coupling coefficients $\kappa_{12}e^{i\phi_{12}} = \kappa_{21}e^{i\phi_{21}}$. The injections $E_{1,inj}(t)$ and $E_{2,inj}(t)$ from the external sources are instantaneous and are multiplied with respective coupling coefficients.

Equations (9)–(10) can be written in the reference frame of the angular frequency ω_{inj} of the external source, which yields equations for the input phase-modulated signals. Equations (9b) and (9d) for N_1 and N_2 do not change, but equations for the slowly varying amplitudes $E_j^{\omega_{inj}}(t) = e^{-it\Delta\omega_{inj}}E_j^{\omega_{fr}}(t)$ and injections $u_j^{\omega_{inj}}(t) = e^{-it\Delta\omega_{inj}}u_j^{\omega_{fr}}(t)$, $j = 1, 2$, become

$$\begin{aligned}\gamma_c^{-1}\dot{E}_1^{\omega_{inj}}(t) = {} & (1+i\alpha)(N_1(t)-1)E_1^{\omega_{inj}}(t) \\ & - i\Delta\omega_{inj}\gamma_c^{-1}E_1^{\omega_{inj}}(t) + u_1^{\omega_{inj}}(t), \qquad (11a)\\ \gamma_c^{-1}\dot{E}_2^{\omega_{inj}}(t) = {} & (1+i\alpha)(N_2(t)-1)E_2^{\omega_{inj}}(t) \\ & - i\Delta\omega_{inj}\gamma_c^{-1}E_2^{\omega_{inj}}(t) + u_2^{\omega_{inj}}(t), \qquad (11b)\end{aligned}$$

and

$$\begin{aligned}u_1^{\omega_{inj}}(t) = {} & \kappa_{12}e^{i\phi_{12}}e^{-i\tau_{12}\Delta\omega_{inj}}E_2^{\omega_{inj}}(t-\tau_{12}) \\ & + \kappa_{1,inj}E_{1,inj}(t), \qquad (12a)\\ u_2^{\omega_{inj}}(t) = {} & \kappa_{21}e^{i\phi_{21}}e^{-i\tau_{12}\Delta\omega_{inj}}E_1^{\omega_{inj}}(t-\tau_{12}) \\ & + \kappa_{2,inj}E_{2,inj}(t). \qquad (12b)\end{aligned}$$

Note that in addition to the optical phase shifts ϕ_{12} and ϕ_{21} in (12), there is also an effective phase shift due to the terms $\exp(-i\tau_{12}\Delta\omega_{inj})$.

Appendix B
Mathematical Analysis of the Steady States of the Memory Circuit

Let us consider the rate equations (6) with zero detuning, i.e., $\Delta\omega_{inj} = 0$, and let us denote $E(t) := E^{\omega_{fr}}(t)$. If the injected field $u \in \mathbb{C}\setminus\{0\}$ is independent of time and small, then the system has a steady state with electric field [59], [61]

$$E = e^{i\theta}\sqrt{\mu-1}\,(u)^0 + O(|u|). \qquad (13)$$

Here $(z)^0 := z/|z|$, $z \in \mathbb{C}\setminus\{0\}$, is the normalization operation, $\theta := -\arg(1+i\alpha)$, and $O(u)$ denotes a function of u with absolute value bounded from the above with some constant multiple of $|u|$.

We consider a simplified model of the memory circuit described by (9) and (10) in its hold-state, i.e., when the external injections $E_{1,inj}$ and $E_{2,inj}$ are independent of time and equal. We denote $E_{inj} = E_{1,inj}$ and we assume $E_{inj} \geq 0$. We choose $\kappa_{12} = \kappa_{21}$ and $\kappa_{1,inj} = \kappa_{2,inj}$, we denote them by κ and κ_{inj}, respectively. We assume that $\kappa > 0$ and $\kappa_{inj} > 0$ are small enough so that we can approximate the steady state electric field of the injection locked lasers by

$$E_k = e^{i\theta}\sqrt{\mu-1}\,(u_k)^0,\ k = 1, 2. \qquad (14)$$

In other words, we drop the small $O(|u|)$-term in (13). Furthermore, we choose $\phi_{12} = \phi_{21} = \pi - \theta$.

Under the approximation (14) and with the above choices for the parameters in (9) and (10), we see that if the memory circuit has stabilized into a steady state, then the electric fields E_1 and E_2 of laser 1 and laser 2, respectively, must satisfy

$$E_1 = e^{i\theta}\sqrt{\mu-1}\,\left(-\kappa e^{-i\theta}E_2 + \kappa_{inj}E_{inj}\right)^0, \qquad (15a)$$

$$E_2 = e^{i\theta}\sqrt{\mu-1}\,\left(-\kappa e^{-i\theta}E_1 + \kappa_{inj}E_{inj}\right)^0. \qquad (15b)$$

System (15) can be solved analytically:

Proposition 1: Let $\mathcal{S} \subset (\mathbb{C}\setminus\{e^{i\theta}\kappa_{inj}E_{inj}/\kappa\})^2$ be the set of solutions of system (15), i.e., the set of steady states of the memory circuit. Define $r = \sqrt{\mu-1}$, and if $\kappa_{inj}E_{inj} \leq 2\kappa\sqrt{\mu-1}$, then define also

$$\Omega := \arg\left(\frac{\kappa_{inj}E_{inj}}{\kappa\sqrt{\mu-1}} + i\sqrt{4-\left(\frac{\kappa_{inj}E_{inj}}{\kappa\sqrt{\mu-1}}\right)^2}\right).$$

1) If $\kappa_{inj}E_{inj} \geq 2\kappa\sqrt{\mu-1}$, then
$$\mathcal{S} = \left\{\left(re^{i\theta}, re^{i\theta}\right)\right\}.$$
2) If $\kappa\sqrt{\mu-1} < \kappa_{inj}E_{inj} < 2\kappa\sqrt{\mu-1}$, then
$$\mathcal{S} = \left\{\left(re^{i(\theta+\Omega)}, re^{i(\theta-\Omega)}\right), \left(re^{i(\theta-\Omega)}, re^{i(\theta+\Omega)}\right), \left(re^{i\theta}, re^{i\theta}\right)\right\}.$$
3) If $\kappa_{inj}E_{inj} = \kappa\sqrt{\mu-1}$, then
$$\mathcal{S} = \left\{\left(re^{i(\theta+\pi/3)}, re^{i(\theta-\pi/3)}\right), \left(re^{i(\theta-\pi/3)}, re^{i(\theta+\pi/3)}\right)\right\}.$$
4) If $0 < \kappa_{inj}E_{inj} < \kappa\sqrt{\mu-1}$, then
$$\mathcal{S} = \left\{\left(re^{i(\theta+\Omega)}, re^{i(\theta-\Omega)}\right), \left(re^{i(\theta-\Omega)}, re^{i(\theta+\Omega)}\right), \left(re^{i\theta}, -re^{i\theta}\right), \left(-re^{i\theta}, re^{i\theta}\right)\right\}.$$
5) If $E_{inj} = 0$, then
$$\mathcal{S} = \left\{(a, -a) \in \mathbb{C}^2 : |a| = r\right\}.$$

Proof: We start by reducing (15) to a simpler system. Define

$$b := (\mu-1)^{-1/2}\kappa_{inj}E_{inj}/\kappa, \qquad (16)$$

and given $E_1, E_2 \in \mathbb{C}\setminus\{e^{i\theta}\kappa_{inj}E_{inj}/\kappa\}$, define

$$z_k := e^{-i\theta}(\mu-1)^{-1/2}E_k \in \mathbb{C}\setminus\{b\},\ k = 1, 2.$$

Then (E_1, E_2) solves system (15), if and only if (z_1, z_2) solves

$$z_1 = (b - z_2)^0, \qquad (17a)$$

$$z_2 = (b - z_1)^0. \qquad (17b)$$

Note that the five order relations between $\kappa_{inj}E_{inj}$ and $\kappa\sqrt{\mu-1}$ in the statement of the proposition correspond to $b \geq 2$, $1 < b < 2$, $b = 1$, $0 < b < 1$, and $b = 0$.

Let (E_1, E_2) be a solution of system (15), and let (z_1, z_2) and b be defined as above. Then

$$|z_1| = |z_2| = 1. \tag{18}$$

We will show that $(E_1, E_2) \in \mathcal{S}$. If $b = 0$ this is clear, so we assume $b \neq 0$. Because

$$|b - z_j|\, z_k = b - z_j,\ j \neq k, \tag{19}$$

and b is real, we have

$$|b - z_j|\ \mathrm{Im}(z_k) = -\mathrm{Im}(z_j),\ j \neq k, \tag{20}$$

and therefore

$$|b - z_1|\,|b - z_2|\,\mathrm{Im}(z_1)\,\mathrm{Im}(z_2) = \mathrm{Im}(z_1)\,\mathrm{Im}(z_2). \tag{21}$$

From (20) it follows in particular that $\mathrm{Im}(z_1) = 0$ if and only if $\mathrm{Im}(z_2) = 0$.

First suppose that z_1 and z_2 are real. By (18) there are only four possible values for (z_1, z_2). Considering the cases $b > 1$, $b = 1$, and $0 < b < 1$ separately shows that necessarily $(E_1, E_2) \in \mathcal{S}$.

It remains to consider the case where z_1 and z_2 both have a nonzero imaginary part. In this case $|b - z_1|\,|b - z_2| = 1$ by (21), together with (19) this implies

$$z_1\, z_2 = (b - z_1)(b - z_2),$$

so

$$z_1 + z_2 = b.$$

Because b is real, we know that $\mathrm{Im}(z_1) = -\mathrm{Im}(z_2)$. It follows that $|\,\mathrm{Re}(z_1)| = |\,\mathrm{Re}(z_2)|$, so $0 < |b| \leq 2$, and

$$\mathrm{Re}(z_1) = \mathrm{Re}(z_2) = b/2 := x. \tag{22}$$

Therefore $|\,\mathrm{Im}(z_k)| = \sqrt{1 - x^2} =: y$, and

$$\arg(z_k) = \arg(x\ \pm iy) = \pm\Omega.$$

This implies that also in this case $(E_1, E_2) \in \mathcal{S}$ (note that $\Omega = \pi/3$ if $b = 1$).

On the other hand, a straightforward verification shows that in each of the five cases all elements of $\mathcal{S}$ solve system (15). ■

REFERENCES

[1] H. J. Schulte and A. J. Rack, "Optical delay line memory," *IEEE J. Quantum Electron.*, vol. 3, no. 6, pp. 246–246, Jun. 1967.

[2] L. Liu et al., "An ultra-small, low-power, all-optical flip-flop memory on a silicon chip," *Nature Photon.*, vol. 4, no. 3, pp. 182–187, 2010.

[3] E. Kuramochi et al., "Large-scale integration of wavelength-addressable all-optical memories on a photonic crystal chip," *Nature Photon.*, vol. 8, pp. 474–481, 2014.

[4] A. Trita, G. Mezōsi, M. Sorel, and G. Giuliani, "All-optical toggle flip-flop based on monolithic semiconductor ring laser," *IEEE Photon. Technol. Lett.*, vol. 26, no. 1, pp. 96–99, Jan. 2014.

[5] T. Moschos et al., "Monolithically integrated InP bistable photonic waveguide memory," *IEEE Photon. Technol. Lett.*, vol. 33, no. 22, pp. 1274–1277, Nov. 2021.

[6] D. K. Hunter, M. C. Chia, and I. Andonovic, "Buffering in optical packet switches," *J. Lightw. Technol.*, vol. 16, pp. 2081–2091, Dec. 1998.

[7] R. S. Tucker, P. C. Ku, and C. J. Chang-Hasnain, "Slow-light optical buffers: Capabilities and fundamental limitations," *J. Lightw. Technol.*, vol. 23, pp. 4046–4066, 2005.

[8] E. F. Burmeister, D. J. Blumenthal, and J. Bowers, "A comparison of optical buffering technologies," *Opt. Switching Netw.*, vol. 5, pp. 10–18, 2008.

[9] D. Apostolopoulos et al., "Contention resolution for burst-mode traffic using integrated SOA-MZI gate arrays and self-resetting optical flip-flops," *IEEE Photon. Technol. Lett.*, vol. 20, pp. 2024–2026, Dec. 2008.

[10] L. M. Augustin et al., "InP-based generic foundry platform for photonic integrated circuits," *IEEE J. Sel. Top. Quant. Electron.*, vol. 24, no. 1, pp. 1–10, Jan.–Feb. 2018.

[11] V. Stojanović et al., "Monolithic silicon-photonic platforms in state-of-the-art CMOS SOI processes," *Opt. Exp.*, vol. 26, pp. 13106–13121, 2018.

[12] Y. Jiao et al., "InP membrane integrated photonics research," *Semicond. Sci. Technol.*, vol. 36, 2020, Art. no. 013001.

[13] Z. Yan et al., "A monolithic InP/SOI platform for integrated photonics," *Light Sci. Appl.*, vol. 10, 2021, Art. no. 200.

[14] D. A. B. Miller, "Are optical transistors the logical next step?," *Nat. Photon.*, vol. 4, pp. 3–5, 2010.

[15] T. Alexoudi, G. T. Kanellos, and N. Pleros, "Optical RAM and integrated optical memories: A survey," *Light Sci. Appl.*, vol. 9, 2020, Art. no. 91.

[16] G. Berrettini et al., "All-optical digital circuits exploiting SOA-based loop memories," *IEEE J. Sel. Top. Quant. Electron.*, vol. 18, no. 2, pp. 847–858, Mar.–Apr. 2012.

[17] A. Malacarne, A. Bogoni, and L. Poti, "Erbium–ytterbium-doped fiber-based optical flip-flop," *IEEE Photon. Technol. Lett.*, vol. 19, no. 12, pp. 904–906, Jun. 2007.

[18] L. Poti, "Erbium-based photonic flip-flop memories: Model and experimental validation," *IEEE J. Quantum Electron.*, vol. 44, no. 5, pp. 473–479, May 2008.

[19] T. Gregorkiewicz et al., "Er-doped electro-optical memory element for 1.5-μm silicon photonics," *IEEE J. Sel. Top. Quant. Electron.*, vol. 12, no. 6, pp. 1539–1544, Nov./Dec. 2006.

[20] M. T. Hill, H. D. Waardt, G. D. Khoe, and H. J. S. Dorren, "Fast optical flip-flop by use of Mach–Zehnder interferometers," *Microw. Opt. Technol. Lett.*, vol. 31, no. 6, pp. 411–415, 2001.

[21] N. Pleros, D. Apostolopoulos, D. Petrantonakis, C. Stamatiadis, and H. Avramopoulos, "Optical static RAM cell," *IEEE Photon. Technol. Lett.*, vol. 21, no. 2, pp. 73–75, Jan. 2009.

[22] S. Pitris et al., "WDM-enabled optical ram at 5 gb/s using a monolithic InP flip-flop chip," *IEEE Photon. J.*, vol. 8, no. 2, Apr. 2016, Art. no. 0600207.

[23] A. Tsakyridis, T. Alexoudi, A. Miliou, N. Pleros, and C. Vagionas, "10 gb/s optical random access memory (RAM) cell," *Opt. Lett.*, vol. 44, no. 7, pp. 1821–1824, 2019.

[24] C. Vagionas, D. Fitsios, G. T. Kanellos, N. Pleros, and A. Miliou, "Optical ram and flip-flops using bit-input wavelength diversity and SOA-XGM switches," *J. Lightw. Technol.*, vol. 30, no. 18, pp. 3003–3009, Sep. 2012.

[25] H. J. S. Dorren, D. Lenstra, Y. Liu, M. T. Hill, and G.-D. Khoe, "Nonlinear polarization rotation in semiconductor optical amplifiers: Theory and application to all-optical flip-flop memories," *IEEE J. Quantum Electron.*, vol. 39, no. 1, pp. 141–148, Jan. 2003.

[26] R. Clavero, F. Ramos, J. M. Martinez, and J. J. Marti, "All-optical flip-flop based on a single SOA-MZI," *IEEE Photon. Technol. Lett.*, vol. 17, no. 4, pp. 843–845, Apr. 2005.

[27] P. Bakopoulos et al., "All-optical t-flip-flop using a single SOA-MZI-based latching element," *IEEE Photon. Technol. Lett.*, vol. 24, no. 9, pp. 748–750, May 2012.

[28] Y. Naito, S. Shimizu, T. Kato, K. Kobayashi, and H. Uenohara, "Investigation of all-optical latching operation of a monolithically integrated SOA-MZI with a feedback loop," *Opt. Exp.*, vol. 20, no. 26, pp. B339–B349, 2012.

[29] M. T. Hill, H. D. Waardt, G. D. Khoe, and H. J. S. Dorren, "All-optical flip-flop based on coupled laser diodes," *IEEE J. Quantum Electron.*, vol. 37, no. 3, pp. 405–413, Mar. 2001.

[30] E. Tangdiongga et al., "Optical flip-flop based on two-coupled mode-locked ring lasers," *IEEE Photon. Technol. Lett.*, vol. 17, no. 1, pp. 208–210, Jan. 2005.

[31] J. Wang, G. Meloni, G. Berrettini, L. Poti, and A. Bogoni, "All-optical clocked flip-flops and binary counting operation using SOA-based SR latch and logic gates," *IEEE J. Sel. Top. Quantum Electron.*, vol. 16, no. 5, pp. 1486–1494, Sep./Oct. 2010.

[32] J. Wang et al., "SOA fiber ring laser-based three-state optical memory," *IEEE Photon. Technol. Lett.*, vol. 20, no. 20, pp. 1697–1699, Oct. 2008.

[33] S. Zhang et al., "Ring-laser optical flip-flop memory with single active element," *IEEE J. Sel. Top. Quantum Electron.*, vol. 10, no. 5, pp. 1093–1100, Sep./Oct. 2004.

[34] C. Harder, K. Y. Lau, and A. Yariv, "Bistability and pulsations in CW semiconductor lasers with a controlled amount of saturable absorption," *Appl. Phys. Lett.*, vol. 39, no. 5, pp. 382–384, 1981.

[35] M. Takenaka and Y. Nakano, "Realization of all-optical flip-flop using directionally coupled bistable laser diode," *IEEE Photon. Technol. Lett.*, vol. 16, no. 1, pp. 45–47, Jan. 2004.
[36] M. Takenaka, M. Raburn, and Y. Nakano, "All-optical flip-flop multimode interference bistable laser diode," *IEEE Photon. Technol. Lett.*, vol. 17, no. 5, pp. 968–970, May 2005.
[37] K. Takeda, Y. Kanema, M. Takenaka, T. Tanemura, and Y. Nakano, "Polarization-insensitive all-optical flip-flop using tensile-strained multiple quantum wells," *IEEE Photon. Technol. Lett.*, vol. 20, no. 22, pp. 1851–1853, Nov. 2008.
[38] Y. D. Jeong, J. S. Cho, Y. H. Won, H. J. Lee, and H. Yoo, "All-optical flip-flop based on the bistability of injection locked Fabry-Perot laser diode," *Opt. Exp.*, vol. 14, no. 9, pp. 4058–4063, 2006.
[39] K. Huybrechts, G. Morthier, and R. Baets, "Fast all-optical flip-flop based on a single distributed feedback laser diode," *Opt. Exp.*, vol. 16, no. 15, pp. 11405–11410, 2008.
[40] W. D'Oosterlinck et al., "All-optical flip-flop operation using a SOA and DFB laser diode optical feedback combination," *Opt. Exp.*, vol. 15, no. 10, pp. 6190–6199, 2007.
[41] G. Yuan, Z. Wang, B. Li, M. I. Memon, and S. Yu, "Theoretical and experimental studies on bistability in semiconductor ring lasers with two optical injections," *IEEE J. Sel. Top. Quantum Electron.*, vol. 14, no. 3, pp. 903–910, May/Jun. 2008.
[42] M. T. Hill et al., "A fast low-power optical memory based on coupled micro-ring lasers," *Nature*, vol. 432, no. 7014, pp. 206–209, 2004.
[43] C.-H. Chen et al., "All-optical memory based on injection-locking bistability in photonic crystal lasers," *Opt. Exp.*, vol. 19, no. 4, pp. 3387–3395, 2011.
[44] D. Fitsios et al., "Ultra-compact III–V-on-Si photonic crystal memory for flip-flop operation at 5 Gb/s," *Opt. Exp.*, vol. 24, no. 4, pp. 4270–4277, 2016.
[45] T. Alexoudi et al., "III–V-on-Si photonic crystal nanocavity laser technology for optical static random access memories," *IEEE J. Sel. Top. Quantum Electron.*, vol. 22, no. 6, pp. 295–304, Nov./Dec. 2016.
[46] A. Shinya et al., "All-optical on-chip bit memory based on ultra high q InGaAsP photonic crystal," *Opt. Exp.*, vol. 16, no. 23, pp. 19382–19387, 2008.
[47] K. Nozaki et al., "Ultralow-power all-optical RAM based on nanocavities," *Nature Photon.*, vol. 6, no. 4, pp. 248–252, 2012.
[48] E. Kuramochi et al., "Ultralow bias power all-optical photonic crystal memory realized with systematically tuned L3 nanocavity," *Appl. Phys. Lett.*, vol. 107, no. 22, 2015, Art. no. 221101.
[49] J. Sakaguchi, T. Katayama, and H. Kawaguchi, "All-optical memory operation of 980-nm polarization bistable VCSEL for 20-Gb/s PRBS RZ and 40-Gb/s NRZ data signals," *Opt. Exp.*, vol. 18, no. 12, pp. 12362–12370, 2010.
[50] T. Katayama, T. Ooi, and H. Kawaguchi, "Experimental demonstration of multi-bit optical buffer memory using 1.55-μm polarization bistable vertical-cavity surface-emitting lasers," *IEEE J. Quantum Electron.*, vol. 45, no. 11, pp. 1495–1504, Nov. 2009.
[51] S. H. Lee et al., "1-GHz all-optical flip-flop operation of conventional cylindrical-shaped single-mode VCSELs under low-power optical injection," *IEEE Photon. Technol. Lett.*, vol. 22, no. 23, pp. 1759–1761, Dec. 2010.
[52] D. Hayashi, H. Takahashi, T. Katayama, and H. Kawaguchi, "Bit error rate measurements of all-optical flip-flop operations of a 1.55-μm polarization bistable VCSEL," *J. Lightw. Technol.*, vol. 32, no. 15, pp. 2671–2677, Aug. 2014.
[53] C. Ríos et al., "Integrated all-photonic non-volatile multi-level memory," *Nature Photon.*, vol. 9, no. 11, pp. 725–732, 2015.
[54] Z. Cheng et al., "Device-level photonic memories and logic applications using phase-change materials," *Adv. Mater.*, vol. 30, no. 32, 2018, Art. no. 1802435.
[55] T. Kakitsuka et al., "Injection-locked flip-flop operation of a DBR laser," *IEEE Photon. Technol. Lett.*, vol. 23, no. 17, pp. 1261–1263, Sep. 2011.
[56] Y. Wu, Y. Zhu, X. Liao, J. Meng, and J.-J. He, "All-optical flip-flop operation based on bistability in V-cavity laser," *Opt. Exp.*, vol. 24, no. 12, pp. 12507–12514, 2016.
[57] N. L. Hoang, J. S. Cho, Y. H. Won, and Y. D. Jeong, "All-optical flip-flop with high on-off contrast ratio using two injection-locked single-mode fabry-perot laser diodes," *Opt. Exp.*, vol. 15, no. 8, pp. 5166–5171, 2007.
[58] J. M. Kahn and K.-P. Ho, "Spectral efficiency limits and modulation/detection techniques for DWDM systems," *IEEE J. Sel. Top. Quantum Electron.*, vol. 10, no. 2, pp. 259–272, Mar./Apr. 2004.
[59] T. von Lerber et al., "All-optical majority gate based on an injection-locked laser," *Sci. Rep.*, vol. 9, no. 1, pp. 1–7, 2019.
[60] N. Li, H. Susanto, B. R. Cemlyn, I. D. Henning, and M. J. Adams, "Locking bandwidth of two laterally-coupled semiconductor lasers subject to optical injection," *Sci. Rep.*, vol. 8, no. 1, pp. 1–10, 2018.
[61] L. Ylinen, T. von Lerber, F. Küppers, and M. Lassas, "Analysis of a dynamical system modeling lasers and applications for optical neural networks," *SIAM J. Appl. Dyn. Syst.*, vol. 21, no. 2, pp. 840–878, 2022. [Online]. Available: https://doi.org/10.1137/21M1405976
[62] J. Martin-Regalado, F. Prati, M. S. Miguel, and N. Abraham, "Polarization properties of vertical-cavity surface-emitting lasers," *IEEE J. Quantum Electron.*, vol. 33, no. 5, pp. 765–783, May 1997.
[63] K. Kikuchi, "Coherent optical communications: Historical perspectives and future directions," in *High Spectral Density Optical Communication Technologies*, (Optical and Fiber Communications Reports Series) M. Nakazawa, K. Kikuchi, and T. Miyazaki, Eds. Berlin, Heidelberg: Springer, 2010, pp. 11–49.
[64] J. Bezanson, A. Edelman, S. Karpinski, and V. B. Shah, "Julia: A fresh approach to numerical computing," *SIAM Rev.*, vol. 59, no. 1, pp. 65–98, 2017.
[65] "DifferentialEquations.jl: Delay differential equations tutorial," 2021. Accessed: Aug. 17, 2021. https://diffeq.sciml.ai/stable/tutorials/dde_example/
[66] E. K. Lau, L. J. Wong, and M. C. Wu, "Enhanced modulation characteristics of optical injection-locked lasers: A tutorial," *IEEE J. Sel. Top. Quantum Electron.*, vol. 15, no. 3, pp. 618–633, May/Jun. 2009.
[67] F. Kano et al., "Linewidth enhancement factor in InGaAsP/lnP modulation-doped strained multiple-quantum-well lasers," *IEEE J. Quantum Electron.*, vol. 30, no. 2, pp. 533–537, Feb. 1994.
[68] A. Fragkos, A. Bogris, D. Syvridis, and R. Phelan, "Colorless regenerative amplification of constant envelope phase-modulated optical signals based on injection-locked Fabry-Pérot lasers," *IEEE Photon. Technol. Lett.*, vol. 24, no. 1, pp. 28–30, Jan. 2012.
[69] K. Ding et al., "Record performance of electrical injection sub-wavelength metallic-cavity semiconductor lasers at room temperature," *Opt. Exp.*, vol. 21, no. 4, pp. 4728–4733, 2013.

Tuomo von Lerber received the Ph.D. degree in technology from Aalto University, Espoo, Finland, in 2007. He has worked in various roles in industry and academia throughout his career. Currently, he is employed by Microsoft, Finland, yet, this Paper relates to his earlier academic activities. His research interests include various aspects of optical computing, in particular, optical logic gates, optical memory, and optical neural networks. Dr. von Lerber has been a Member of Optica (formerly OSA) since 2003.

Vladimir S. Lyubopytov received the graduation degree (*cum laude*) with the qualification of Engineer in multichannel telecommunication systems, and the Candidate of Sciences degree in systems, networks and devices of telecommunications from Ufa State Aviation Technical University, Ufa, Russia, in 2008 and 2013, respectively.

Since 2012, he has been a Researcher with Ufa State Aviation Technical University, during 2015–2016, he was a Visiting Researcher with the Institute for Microwave Engineering and Photonics (IMP), TU Darmstadt, Darmstadt, Germany, from 2016 to 2018 he was a Postdoc with DTU Fotonik, Technical University of Denmark, Denmark. Since 2020, he has been a Senior Researcher with the Center for Photonic Science and Engineering, Skolkovo Institute of Science and Technology, Moscow, Russia. His research interests include the high-speed optical communications, digital and optical signal processing, integrated photonics.

Lauri Ylinen received the M.Sc. (Eng.) degree in mathematics from the Tampere University of Technology, Tampere, Finland, in 2005. Since 2017 he has been working toward the Ph.D. degree with the University of Helsinki, Helsinki, Finland. His research interests include inverse problems and dynamical systems.

Matti Lassas received the Ph.D. degree in mathematics from the University of Helsinki, Helsinki, Finland, in 1996. Between 2004 and 2008, he was a Professor of mathematics with the Helsinki University of Technology, Espoo, Finland, and in 2010, a Research Professor with Mathematical Sciences Research Institutewith the University of California, Berkeley, Berkeley, CA, USA. Since 2009 he has been a Professor of applied mathematics with Department of Mathematics and Statistics, University of Helsinki. He is the Director of the Centre of Excellence on Inverse Modelling and Imaging, funded by the Academy of Finland. His research interests include inverse problems, imaging applications, machine learning and mathematical methods on electromagnetism, in particular, differential geometrical methods on these subjects. He has also studied metamaterials and invisibility cloaking for electromagnetic and quantum fields and dynamical systems related to lasers.

Franko Küppers received the Ph.D. degree in optical communications engineering from TU Kaiserslautern, Kaiserslautern, Germany, in 2002. He was with Siemens (Erlangen, Germany) and with Deutsche Telekom's R&D Center, Darmstadt, Germany, where he directed the Optical Networks Research Group and the Photonic Systems Department. In 2003, he joined the College of Optical Sciences, University of Arizona, Tucson, AZ, USA, where he was a tenured Associate Professor, built and ran the Photonic Telecommunication Systems Research Group, and was the Testbed Lead for the National Science Foundation's Engineering Research Center for Integrated Access Networks (NSF ERC CIAN) with which he is still associated as an Adjunct Professor. From 2011 to 2018, he directed the Institute for Microwave Engineering and Photonics, TU Darmstadt, Darmstadt, Germany, where he also held the Chair of Photonics and Optical Communications. In 2019, he was appointed a Full Professor and the Director of the Center for Photonics and Quantum Materials, Skolkovo Institute of Science and Technology, Moscow, Russia, the affiliation ended March 2022. He has authored or coauthored more than 200 scientific articles and was the Guest Editor of the IEEE/OSA JOURNAL OF LIGHTWAVE TECHNOLOGY Special Issue on 40 Gb/s Lightwave Systems in 2002. He was the recipient of the NSF CAREER Award, the Science Foundation Arizona Competitive Advantage Award, and the College Award of Distinction for Outstanding Undergraduate Teaching. He is a Fellow of SPIE and a Senior Member of the IEEE Photonics and Communications Section.